

RESEARCH ARTICLE

Induction of stable ER–plasma-membrane junctions by Kv2.1 potassium channels

Philip D. Fox¹, Christopher J. Haberkorn¹, Elizabeth J. Akin¹, Peter J. Seel², Diego Krapf^{2,3} and Michael M. Tamkun^{1,4,*}

ABSTRACT

Junctions between cortical endoplasmic reticulum (cER) and the plasma membrane are a subtle but ubiquitous feature in mammalian cells; however, very little is known about the functions and molecular interactions that are associated with neuronal ER–plasma-membrane junctions. Here, we report that Kv2.1 (also known as KCNB1), the primary delayed-rectifier K⁺ channel in the mammalian brain, induces the formation of ER–plasma-membrane junctions. Kv2.1 localizes to dense, cell-surface clusters that contain non-conducting channels, indicating that they have a function that is unrelated to membrane-potential regulation. Accordingly, Kv2.1 clusters function as membrane-trafficking hubs, providing platforms for delivery and retrieval of multiple membrane proteins. Using both total internal reflection fluorescence and electron microscopy we demonstrate that the clustered Kv2.1 plays a direct structural role in the induction of stable ER–plasma-membrane junctions in both transfected HEK 293 cells and cultured hippocampal neurons. Glutamate exposure results in a loss of Kv2.1 clusters in neurons and subsequent retraction of the cER from the plasma membrane. We propose Kv2.1-induced ER–plasma-membrane junctions represent a new macromolecular plasma-membrane complex that is sensitive to excitotoxic insult and functions as a scaffolding site for both membrane trafficking and Ca²⁺ signaling.

KEY WORDS: Ion channels, Sub-surface cisterns, Membrane contact sites

INTRODUCTION

The endoplasmic reticulum (ER) is the most extensive membranous organelle, containing a single continuous lumen and stretching from the nuclear envelope to the cell cortex in a system of tubules and sheets (cisterns) (English et al., 2009). The ER participates in close connections, or membrane contact sites (MCSs), with nearly every other membranous organelle (Prinz, 2014). MCSs between the ER and plasma membrane – i.e. ER–plasma-membrane junctions – are particularly important for signal transduction because most intracellular signals originate at the plasma membrane and the ER is a Ca²⁺ store that is involved in both the initiation and termination of signaling events (Carrasco and Meyer, 2011). The ER membrane is also a site of lipid synthesis and other enzymatic activity that can act across the membrane junction, and potentially transfer lipids

directly to the plasma membrane (English and Voeltz, 2013; Schauder et al., 2014). ER–plasma-membrane junctions were first discovered in skeletal muscle (Porter and Palade, 1957), where they are necessary for excitation-contraction coupling (Franzini-Armstrong and Jorgensen, 1994). More recently, the interaction of an ER Ca²⁺ sensor, stromal interaction molecule 1 (STIM1), with a plasma membrane Ca²⁺ channel, ORAI1, at ER–plasma-membrane junctions was found to be crucial for Ca²⁺-dependent lymphocyte activation (Hogan et al., 2010). Despite the observation of neuronal ER–plasma-membrane junctions, or sub-surface cisterns (SSCs), as demonstrated by more than 50 years of electron microscopy experiments (Rosenbluth, 1962), little is known about the molecular components involved in neuronal ER–plasma-membrane junction formation, maintenance and function (Helle et al., 2013).

The best indication of the function of neuronal ER–plasma-membrane junctions comes from the identification of the proteins that have localized there. For example, large conductance Ca²⁺-activated K⁺ (BK) channels localize above SSCs in cerebellar purkinje neurons where ER Ca²⁺ release might be coupled to BK channel activation (Kaufmann et al., 2009). Another K⁺ channel that localizes to ER–plasma-membrane junctions (or SSCs) is the primary delayed-rectifier K⁺ channel in the mammalian brain, Kv2.1 (also known as KCNB1). Kv2.1 regulates the action potential frequency in a wide variety of neuronal cell types in the mammalian brain, but it also displays an intriguing membrane localization pattern of micron-sized cell-surface clusters over the soma, proximal dendrites and axon initial segment in the intact brain and in cultured neurons (Lim et al., 2000; Sarmiere et al., 2008). The clustered phenotype can be recapitulated heterologously in transfected HEK cells (O’Connell et al., 2006; Tamkun et al., 2007). Early electron microscopy analyses of Kv2.1 immuno-gold labeling in the hippocampus have indicated that Kv2.1 clusters localize above SSCs that are juxtaposed to astrocytic processes (Du et al., 1998), and fluorescence microscopy analyses of live cultured cells shows that Kv2.1 clusters reside atop projections of the ER that terminate near the plasma membrane – i.e. cortical ER (cER) (Fox et al., 2013a). Consistent with these observations, Kv2.1 clusters on the soma and axon initial segment partially colocalize with ryanodine receptors (RyRs) in culture and in the intact brain (King et al., 2014; Lim et al., 2000; Mandikian et al., 2014). Additionally, somatic Kv2.1 clusters on α -motor neurons localize to cholinergic terminals with underlying SSCs (Muennich and Fyffe, 2004; Nagy et al., 1993).

Although the localization of Kv2.1 to ER–plasma-membrane junctions is well documented, no logical hypothesis as to the purpose of its localization to this specialized structure exists. We have previously demonstrated that the vast majority of clustered Kv2.1 channels are non-conducting with the majority of the K⁺ flux coming from a subpopulation of channels that are diffusely localized over the cell surface (Fox et al., 2013b; O’Connell et al.,

¹Department of Biomedical Sciences, Colorado State University, Fort Collins, CO 80523, USA. ²School of Biomedical Engineering, Colorado State University, Fort Collins, CO 80523, USA. ³Department of Electrical and Computer Engineering, Colorado State University, Fort Collins, CO 80523, USA. ⁴Department of Biochemistry and Molecular Biology, Colorado State University, Fort Collins, CO 80523, USA.

*Author for correspondence (michael.tamkun@colostate.edu)

Received 11 November 2014; Accepted 13 April 2015

2010). Kv2.1 is expressed abundantly in the neuronal soma, suggesting that the channel takes on a non-traditional function that is not related to the regulation of action potentials, which requires a high level of expression – as expected of a structural or scaffolding protein. Indeed, there is a growing list of ion channels that possess functions unrelated to ion conduction (Kaczmarek, 2006). Consistent with this idea, we have recently discovered that in both HEK 293 cells and hippocampal neurons, multiple membrane proteins are preferentially trafficked to and from the plasma membrane at the perimeter of Kv2.1 clusters, suggesting the clusters define cell surface trafficking hubs (Deutsch et al., 2012).

In this report, we use fluorescence and electron microscopy to show that Kv2.1 not only localizes to ER–plasma-membrane junctions but, in fact, induces the formation of these structures through substantial remodeling of the cER. We find that treatment of neurons with glutamate results in a loss of Kv2.1 clusters that is followed by the retraction of cER from the plasma membrane. To the best of our knowledge, Kv2.1 is the first plasma membrane protein that has been identified as governing the formation of ER–plasma-membrane junctions under resting conditions. The presence of non-conducting Kv2.1 channels (Fox et al., 2013b; O’Connell et al., 2010) allows the clusters to achieve the high channel density that is required to induce junction formation without compromising electrical signaling. Given the well-accepted role of ER–plasma-membrane junctions in Ca^{2+} homeostasis in immune cells (Hogan et al., 2010) and that Kv2.1 clusters serve as sites for endo- and exocytosis (Deutsch et al., 2012), the Kv2.1-induced ER–plasma-membrane junctions are proposed to represent a macromolecular complex that functions as a scaffolding site to couple membrane trafficking to Ca^{2+} signaling.

RESULTS

Kv2.1 expression remodels the cER in HEK 293 cells

After transfecting HEK 293 cells (hereafter referred to as HEK cells) with green fluorescent protein (GFP)-tagged Kv2.1 and the luminal ER marker DsRed2-ER, we observed that, in cells expressing only DsRed2-ER, the cER in the total internal reflection illumination field – i.e. within 100 nm of the coverslip – had a very different structure relative to that observed in cells in which Kv2.1 was also expressed. Fig. 1A shows the cER pattern in two distinct HEK cells (which are outlined in white) that had been transfected with both GFP–Kv2.1 and DsRed2-ER, and then imaged by using total internal reflection fluorescence (TIRF) microscopy. Fig. 1B shows that the cell in the upper part of the image received only the DsRed2-ER marker, whereas the cell in the bottom left corner received both plasmids and exhibits large GFP–Kv2.1 clusters. Without Kv2.1, the cER appears as either small puncta (Fig. 1C, yellow arrow) or a meshwork of tubules. In the presence of Kv2.1, the cER was dramatically remodeled (Fig. 1D), and most of the cER appeared as large planar structures (white arrow) beneath the Kv2.1 clusters. Furthermore, the cER that was associated with Kv2.1 clusters was generally brighter than the cER that was not, even within the same cell. This is illustrated by the histogram in Fig. 1E, which shows that the Kv2.1-cluster-associated cER (black boxes, mean±s.e.m.) accounts for the brightest pixels from the total population of cER (red boxes) in cells expressing Kv2.1 ($n=6$). Kv2.1-induced remodeling of the cER was also observed in transfected rat hippocampal neurons after being cultured for 7 days *in vitro* (DIV), a time point at which endogenous Kv2.1 clusters are not yet expressed (Antonucci et al., 2001), as illustrated in Fig. 1F–H. In addition, supplementary material Fig. S1 shows that as rat hippocampal neurons matured in culture and endogenous Kv2.1 expression increased, the tubular cER phenotype transitioned into a planar phenotype that was

characteristic of Kv2.1-induced ER–plasma-membrane junctions. The Kv2.1-remodeled cER pattern in both HEK cells and neurons was reminiscent of the pattern that is induced by expression and activation

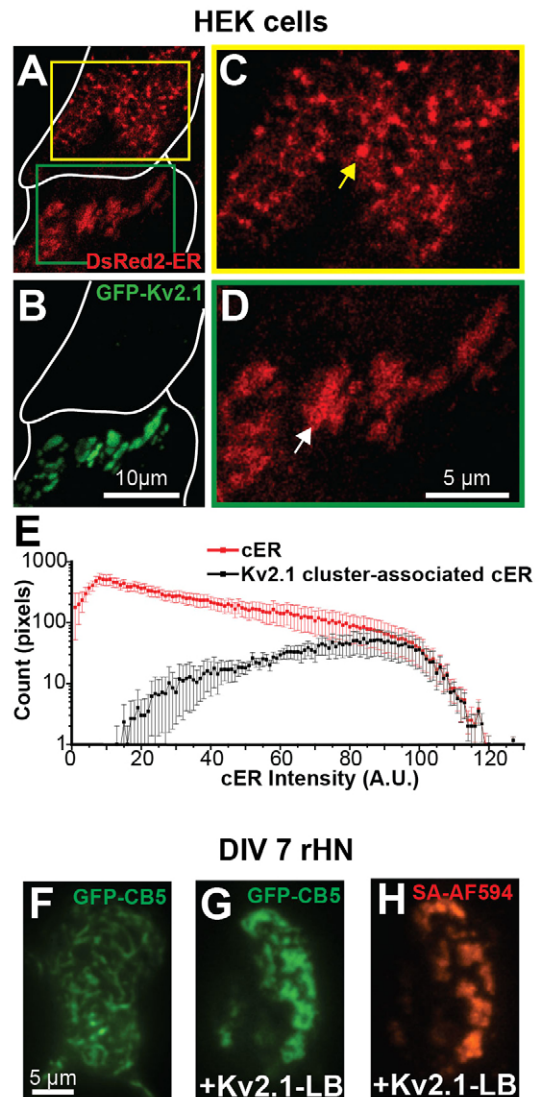


Fig. 1. Clustering of Kv2.1 remodels the cER. Two HEK cells, outlined in white, that had been transfected with the luminal ER marker DsRed2-ER (A) and GFP–Kv2.1 (B) were imaged using TIRF microscopy. The bottom cell has large GFP–Kv2.1 clusters, whereas the top left cell has no Kv2.1 expression. Both cells exhibit similar intensities of DsRed2-ER. (C) Enlargement of the region in the yellow box from A. Note the mesh-like pattern of the cER, which comprises tubules and bright puncta (yellow arrow). (D) Enlargement of the green box in A. Note the absence of mesh-like tubules in favor of large planar cER structures (white arrow). (E) Histogram of the pixel intensities of the entire cER (red boxes) and the Kv2.1-cluster-associated cER (black boxes) obtained from imaging DsRed2-ER in TIRF and averaged over six cells (mean±s.e.m.). The brightest cER pixels were almost exclusively present underneath Kv2.1 clusters, suggesting close proximity to the plasma membrane. (F) Representative 7-DIV rat hippocampal neuron that had been transfected with the membrane domain of cytochrome B5 (CYB5A) fused to GFP (GFP–CB5) and imaged in TIRF. The majority of neurons imaged at this time in culture had apparent tubular cER and small punctate cER but lacked larger cER structures. (G,H) A representative 7-DIV rat hippocampal neuron that had been transfected with GFP–CB5 (G) and Kv2.1-LoopBAD, which comprises an extracellular biotin tag (H, surface labeled with streptavidin–Alexa594). The large, Kv2.1-associated cER structures (G, GFP–CB5) were strikingly different than anything present in 7-DIV neurons that lacked ectopic expression of Kv2.1.

of STIM1, which forms ER–plasma-membrane junctions in response to depletion of ER Ca^{2+} (Wang et al., 2010).

The axial resolution of TIRF imaging is too low to demonstrate that Kv2.1 induces a true ER–plasma-membrane junction with a <20 nm gap between the two membranes (Carrasco and Meyer, 2011; Orci et al., 2009). Thus, in order to examine the spatial relationship between Kv2.1 clusters on the plasma membrane and the underlying cER at high resolution, we used immuno-electron microscopy. HEK cells were either mock transfected (no plasmid DNA) or transfected with a construct encoding Kv2.1 that had an extracellular hemagglutinin tag (Kv2.1–HA), and then fixed with glutaraldehyde. Cells were then labeled with a primary antibody against HA and secondary antibodies conjugated to 10- and 20-nm gold particles before Epon embedding and thin sectioning. The cER in Kv2.1-free HEK cells typically appeared as tubules that approached the plasma membrane but failed to make close (<20 nm) and continuous structures that are characteristic of ER–plasma-membrane junctions. The top-left panel of Fig. 2A shows a fragment of cER that appeared in the proximity of the plasma membrane but lacked the close, evenly spaced gap that is typical of ER–plasma-membrane junctions (Orci et al., 2009). These organelles are likely to correspond to the tubular structures observed in TIRF analyses (Fig. 1C). We also observed small endogenous ER–plasma-membrane junctions (black arrows, top-right and bottom panels of Fig. 2A) that displayed the even, tight contact characteristic of ER–plasma-membrane junctions and that are likely to correspond to the bright puncta which were seen by using TIRF microscopy. By contrast, when Kv2.1–HA was expressed in the HEK cells, we frequently observed larger ER–plasma-membrane contacts where the two membranes were within 10–15 nm of each other over long distances. Fig. 2B shows two representative junctions where the cER made consistent contact with the plasma membrane over almost 1 μm . Multiple 10- and 20-nm gold particles were visible directly over junctional membrane, which confirmed the clustering of Kv2.1 on the plasma membrane. Fig. 2C summarizes the effect of Kv2.1 expression on ER–plasma-membrane junctions in HEK cells. The average length of junctions in cells that showed positive immuno-gold labeling of Kv2.1 was 708 ± 59 nm (mean \pm s.e.m., $n=139$ junctions averaged from 20 cells), which was significantly larger than the size of endogenous junctions in mock-transfected cells (222 ± 9 nm, $n=132$ junctions, 36 cells, $P<0.01$). The proportion of the plasma membrane that involved ER junctions in cells that were positive for Kv2.1 labeling was $20.7 \pm 2.2\%$ versus only $2.8 \pm 0.4\%$ in mock-transfected cells (mean \pm s.e.m., $n=20$ and 36 cells, respectively). The mean distance between the cER and plasma membrane in Kv2.1-positive cells was 15 ± 3 nm (mean \pm s.e.m., $n=30$ junctions). This distance is small enough to allow us to postulate that the cytoplasmic domains of Kv2.1 directly interact with either ER-membrane protein or lipid components. Taken together, the images presented in Figs 1 and 2 indicate that Kv2.1 expression significantly remodels the cER and greatly enhances the surface area of ER–plasma-membrane junctions.

Kv2.1 cluster formation and cER remodeling occur simultaneously

In HEK cells that express GFP–Kv2.1, cell surface clusters are often lost when the cell culture dish is removed from the incubator, the medium is replaced with imaging saline and the dish is placed on the heated TIRF microscope stage. However, after a few minutes, the clusters reform as the dish returns to physiological temperature (37°C). We took advantage of this process to examine the temporal relationship between Kv2.1 cluster formation and cER remodeling

in cells that expressed both GFP–Kv2.1 and the DsRed2-ER marker. As illustrated in Fig. 3A and supplementary material Movie 1, cells that showed a homogenous surface-expression pattern of Kv2.1 at the beginning of imaging had a tubular cER structure within the TIR illumination field, similar to that observed in non-transfected cells (see Fig. 1C). As Kv2.1 clusters reformed and grew over 20 min, the associated cER fluorescence increased (Fig. 3B). As is especially evident in supplementary material Movie 1, the brightest cER puncta served as nucleation sites for Kv2.1-cluster formation. Fig. 3C shows the quantitation of the temporal co-evolution of the six GFP–Kv2.1 clusters from supplementary material Movie 1 and the cER fluorescence beneath these clusters. GFP–Kv2.1-cluster formation and development of the DsRed2-ER-junction fluorescence occurred concurrently, suggesting that cluster

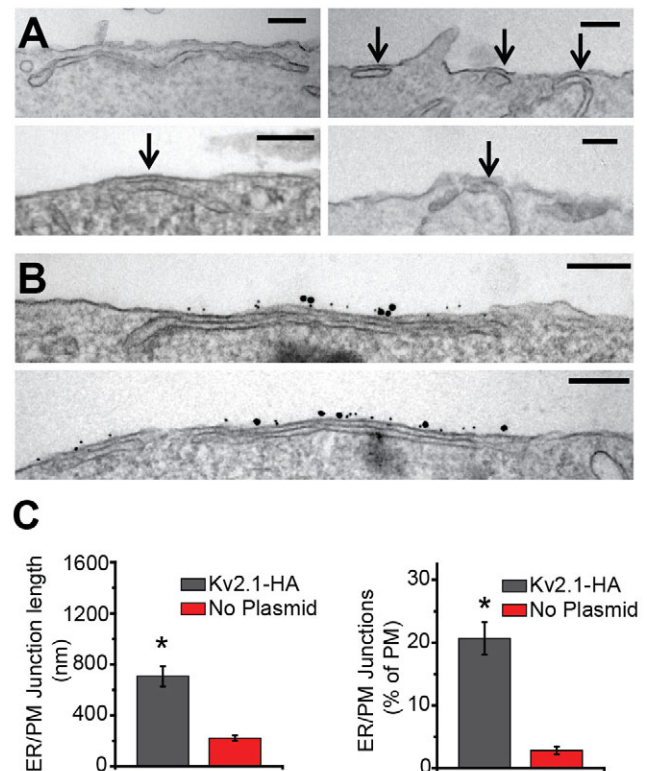


Fig. 2. Kv2.1 clustering induces the formation of true ER–plasma-membrane junctions. Immuno-gold labeling and electron microscopy were used to visualize the ultrastructural features of Kv2.1-remodeled cER. (A) Electron microscopy micrographs of cER from mock-transfected HEK cells. The four micrographs were obtained from cells under identical conditions. Top left panel shows a long stretch of cER that fails to make the consistent close contact that is a hallmark of ER–plasma-membrane junctions. Black arrows in the top-right and bottom panels point to endogenous ER–plasma-membrane junctions, which tended to be ~200 nm in length. (B) Two representative electron microscopy micrographs of long ER–plasma-membrane junctions (~1 μm) in a Kv2.1–HA transfected HEK cell. Kv2.1–HA channels on the cell surface labeled with 10-nm- and 20-nm gold. Scale bars: 200 nm (all electron microscopy micrographs). (C) Bar graphs summarizing the effect of Kv2.1 expression on ER–plasma-membrane junctions in HEK cells. The left-hand graph illustrates the average length of ER–plasma-membrane junctions in cells positive for Kv2.1 by using immuno-gold labeling ($n=139$ junctions averaged from 20 cells) versus mock-transfected cells ($n=132$ junctions averaged from 36 cells). The right-hand graph shows the percentage of the plasma membrane that was associated ER junctions in cells that were positive for immuno-gold labeling of Kv2.1 ($n=20$ cells) versus mock-transfected cells ($n=36$ cells), mean \pm s.e.m., $*P<0.01$.

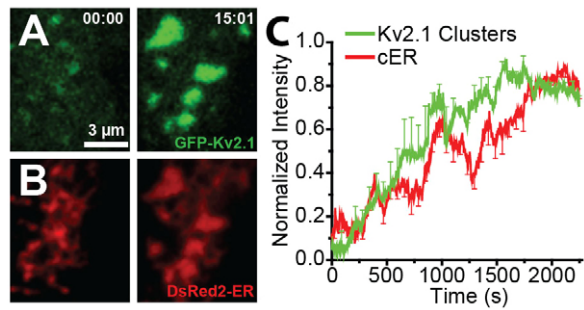


Fig. 3. Clustering of Kv2.1 and formation of ER–plasma-membrane junctions. Transfected HEK cells expressing DsRed2-ER (A) and GFP–Kv2.1 (B) were removed from the incubator, the growth medium was replaced with imaging saline, and the cells were placed on the TIRF microscope stage. Frequently, cells expressing GFP–Kv2.1 initially lacked clusters (A, left panel) and the cER was largely tubular in appearance (B, left panel). Over the next 20 min of imaging, Kv2.1 clusters formed (A, right panel) and the cER remodeled from tubules into larger, planar structures (B, right panel). The time from the start of imaging is shown in the top right of the images in A. (C) The average normalized intensities from six GFP–Kv2.1 clusters (green line) and six cluster-associated cER puncta (red line) during Kv2.1 re-clustering (mean \pm s.e.m.). For intensity measurements, the locations of Kv2.1 clusters and associated cER puncta were automatically tracked using a centroid-based algorithm implemented in LabView. In this cell, the fluorescence intensities of Kv2.1 clusters and cER increased in concert with one another (see supplementary material Movie 1).

formation and direct interaction of Kv2.1 with the ER membrane are closely linked processes. If Kv2.1-cluster formation is first required for the ER to be pulled into close proximity with the plasma membrane, cluster formation should precede the induction of the ER–plasma-membrane junctions. The images presented in Fig. 3 are consistent with a model in which freely diffusing Kv2.1 begins to bind to the cER membrane whenever it is in close proximity with the plasma membrane. The resulting cER tethering at the plasma membrane further enhances Kv2.1 clustering, which in turn leads to enhanced ER–plasma-membrane junction formation.

Kv2.1 stabilizes the associated cER

From the experiment illustrated in supplementary material Movie 1, it appeared that cER that was associated with Kv2.1 clusters was more stable than the rest of the cER, which was likely to be making only sporadic contact with the plasma membrane. Therefore, we examined

the effect of Kv2.1 expression on cER dynamics. HEK cells that had been transfected with GFP–Kv2.1 and DsRed2-ER were mounted onto the microscope stage, and after a few minutes we searched for pairs of cells expressing DsRed2-ER (Fig. 4A) but with only one of them expressing Kv2.1 (lower left, Fig. 4B). Fig. 4D is a kymograph taken from the dashed white line through the top-right cell in Fig. 4A, illustrating the movement that was typical of the cER in HEK cells that expressed only DsRed2-ER. This is in contrast to the kymograph in Fig. 4E, which is taken from Kv2.1-associated cER, corresponding to the white dashed line through the bottom-left cell in Fig. 4A. These lines emphasize the cER edges so that the kymographs are sensitive to cER movement. As indicated in the kymographs, the cER appeared qualitatively more stable in the presence of Kv2.1, as might be expected for cER ‘spot welded’ into true junctions with the plasma membrane. By contrast, the unanchored cytoplasmic cER was more dynamic. In order to quantitate the cER mobility, we employed particle image velocimetry (PIV) analysis (Raffel et al., 2007). In cells that expressed Kv2.1 clusters, the mean velocity of the cER, measured within 0.32-s intervals, was 50 ± 38 nm/s (mean \pm s.d., $n=5$ cells), whereas, in cells expressing only DsRed2-ER, the mean velocity was 69 ± 56 nm/s ($n=6$). Not only were the mean velocities of unanchored cER substantially higher, but their standard deviation was higher as well, which is a consequence of unanchored cER having the ability to move more freely. The proportion of the cER that had velocities smaller than a given value is shown by the cumulative distribution function (CDF) of the velocities in Fig. 4F, which indicates that, as a population, the cER is less dynamic upon interaction with Kv2.1. Such enhanced stability is predicted to provide a sturdy platform for the signaling events that potentially occur at the ER–plasma-membrane junctions.

Glutamate exposure disrupts Kv2.1-induced ER–plasma-membrane junctions

In order to address the relationship between Kv2.1 clustering and the formation of ER–plasma-membrane junctions in a physiologically-relevant environment, we turned to cultured rat hippocampal neurons. Kv2.1 clusters are sensitive to stroke-related insults, such as chemical ischemia and glutamate exposure, both in culture and in the intact brain (Misonou et al., 2005; Misonou et al., 2004; Misonou et al., 2008; Mulholland et al., 2008). Therefore, we used glutamate to induce Kv2.1-cluster dissolution in cultured rat hippocampal neurons and to examine the effect of declustering on the underlying cER. Cultured rat

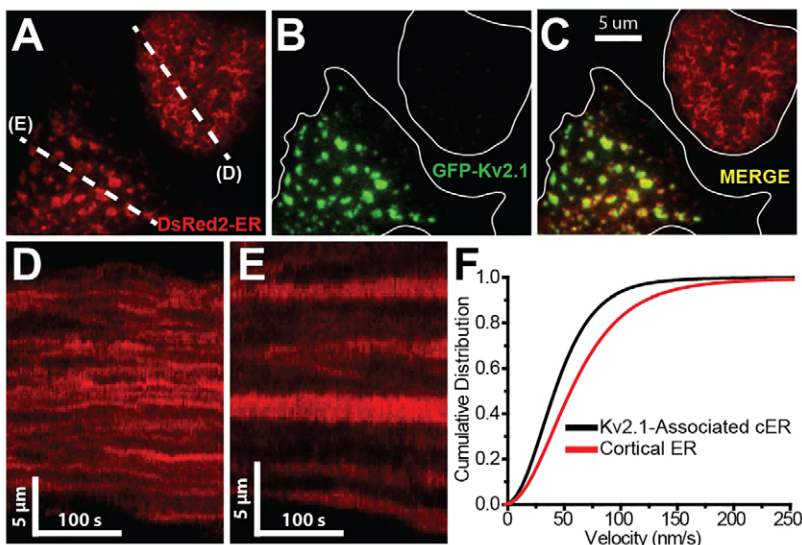


Fig. 4. Kv2.1 clustering enhances the stability of underlying cER. (A) Two HEK cells co-transfected with DsRed2-ER (A, single channel) and GFP–Kv2.1 (B, single channel), imaged in TIRF. The cell on the bottom left has abundant Kv2.1 clusters, whereas the cell in the top right is completely devoid of clustered Kv2.1. ‘(D)’ and ‘(E)’ refer to the respective figure panels. (C) A merge of the two fluorescent channels in A and B, illustrating the association between Kv2.1 clusters and the remodeled cER. The white outlines in B and C indicate cell perimeters. (D) A kymograph generated from the dashed white line through the top-right cell in A, intersecting tubular cER, which shows the movement typical of cER in HEK cells expressing only DsRed2-ER (4 min total). (E) A kymograph generated from the dashed white line through the bottom left cell in A, intersecting Kv2.1-induced ER–plasma membrane junctions, which highlights the long-term stability of these junctions. (F) A cumulative distribution plot of velocities of normal cER (red line) and Kv2.1-associated cER (black line) as measured by particle image velocimetry. As a population, the Kv2.1-associated cER had smaller velocities than the normal cER; hence, the cER is less dynamic upon association with Kv2.1.

hippocampal neurons were transfected with GFP–Kv2.1 and DsRed2-ER, and used for experiments between 8–12 DIV, a time when endogenous Kv2.1 clusters are just beginning to form (Antonucci et al., 2001). These cells showed strong colocalization between Kv2.1 clusters and the cER when imaged using TIRF (Fig. 5A). Cells were imaged for 5–10 min in order to establish a stable baseline before application of 20 μ M glutamate at time=0 s. In the first few minutes following treatment with glutamate, the Kv2.1 clusters dissolved almost entirely (Fig. 5B). This declustering is due to redistribution of the surface Kv2.1 as opposed to internalization (Misonou et al., 2005; Misonou et al., 2004). Although the cER that was associated with Kv2.1 clusters dramatically decreased in size and fluorescence intensity (Fig. 5C), this process occurred more slowly and, typically, did not begin until after the Kv2.1 clusters had been partially dissolved. This phenomenon is illustrated in Fig. 5B–D (magnified regions of the boxed area in Fig. 5A). Given that the concentration of DsRed2 fluorophores within the ER lumen is not expected to change, the decrease in fluorescence intensity suggests that the cER moves away from the TIRF excitation field by retracting away from the plasma membrane. Thus, the loss of Kv2.1 channels from the clusters appears to be correlated to retraction of the cER.

To analyze the temporal relationship between Kv2.1-cluster dissolution and cER retraction, we measured the fluorescence intensity of Kv2.1 and the underlying cER structures from 115 clusters in nine different neurons. The locations and total intensity of Kv2.1 clusters and the underlying cER were measured separately using a centroid-based tracking algorithm implemented in LabView.

Fig. 5E shows a trace from a single cluster taken from the cell shown in Fig. 5A. The beginning of glutamate perfusion is set at time=0 s, and the duration of perfusion is indicated by the black bar (\sim 45 s). The loss in fluorescence of Kv2.1 clusters and cER was observed to start at lag times T_{KV} and T_{ER} after the beginning of treatment with glutamate, which is indicated in Fig. 5E by the green and red arrowheads, respectively. After the onset of fluorescence loss, the intensity of both the Kv2.1 clusters and the cER follows a single exponential decay for several minutes. Thus, the rate of fluorescence loss is characterized by a single time τ . As shown in Fig. 5E, τ is found from an exponential fit (diagonal dashed lines):

$$I(t) = \exp[-(t - T)/\tau], \quad (1)$$

where T is the lag time and τ is the characteristic fluorescence decay time for either Kv2.1 or ER. Eqn 1 holds for both Kv2.1 and ER, albeit with different parameters. Fig. 5F shows the mean \pm s.e.m. of the lag times (T_{KV} and T_{ER}) and decay times (τ_{KV} and τ_{ER}). Kv2.1 clusters began dissolving an average of $T_{KV}=59\pm 5$ s after the initial application of glutamate, whereas the associated cER began losing fluorescence consistently later ($T_{ER}=164\pm 14$ s). The rate at which Kv2.1 cluster fluorescence decreased was also significantly faster than the associated cER ($\tau_{KV}=172\pm 7$ s, $\tau_{ER}=411\pm 19$ s). Fig. 5G shows a scatter plot of T_{ER} against τ_{KV} , where each individual point is a Kv2.1-cluster–cER pair. Here, a positive correlation between the onset of cER retraction and the loss of Kv2.1 clusters was confirmed by the Pearson's correlation coefficient $r=0.5$ (Fig. 5I). In other words, the faster Kv2.1 clusters dissolved, the more rapidly the cER started retracting. Fig. 5H displays a scatter plot of τ_{KV} vs. τ_{ER} where there was no evident correlation

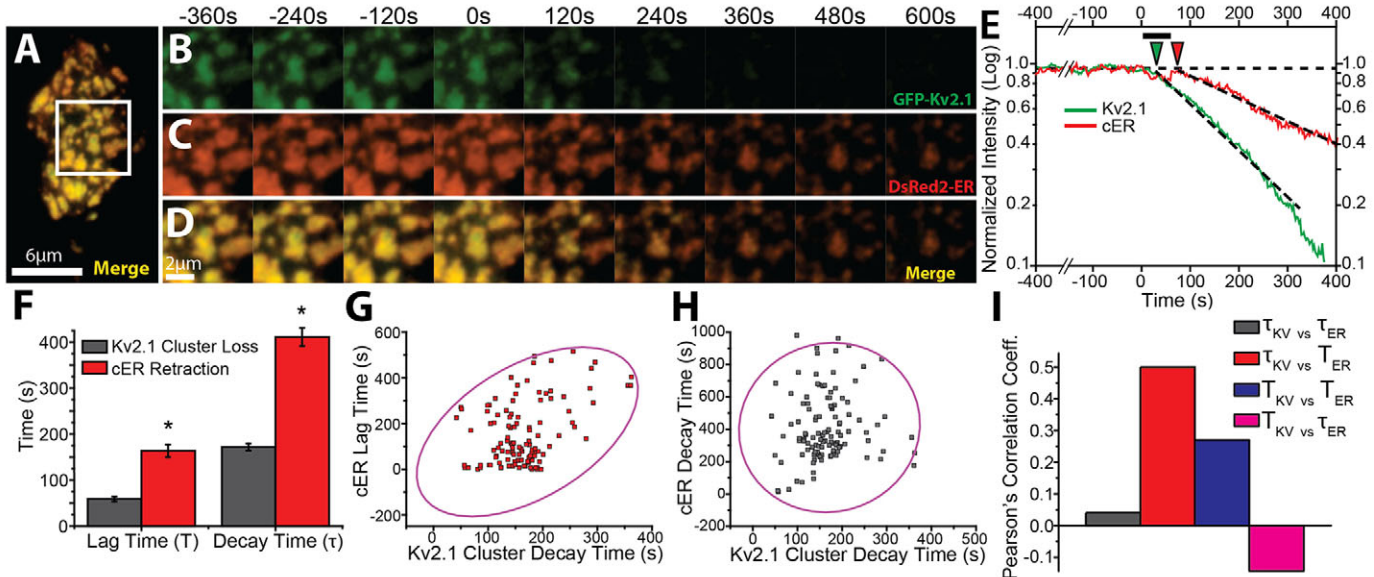


Fig. 5. Kv2.1-induced ER–plasma-membrane junctions are sensitive to glutamate exposure in neurons. The effect of exposure to glutamate (Glut, 20 μ M) was studied in 10-DIV rat hippocampal neurons that had been transfected with GFP–Kv2.1 and DsRed2-ER, and then imaged in TIRF to visualize the Kv2.1-induced ER–plasma-membrane junctions. (A) A representative neuron illustrating perfect colocalization between GFP–Kv2.1 and DsRed2-ER. (B–D) Panels are magnified from the white box in A and contain a series of images over the course of glutamate exposure (beginning at 0 s). GFP was lost from clusters following glutamate exposure as channels diffused out of the clusters, whereas the DsRed2-ER signal was lost as the cER moved away from the plasma membrane towards the interior of the cell. (E) A representative trace of the normalized fluorescence intensity of an individual cER–Kv2.1 cluster pair plotted on a Log_{10} scale. The black bar indicates the duration of perfusion of 20 μ M glutamate and the green (Kv2.1) and red (ER) arrowheads denote the time difference between glutamate perfusion and the initial decrease in fluorescence (lag times, T_{KV} and T_{ER}). The dashed lines denote the area of each trace used for a linear fit of $I(t) = \exp[-(t - T)/\tau]$ from which we extracted characteristic fluorescence decay times (τ_{KV} and τ_{ER}). (F) Bar graphs summarizing the average lag times (T_{KV} and T_{ER}), and decay times (τ_{KV} and τ_{ER}) (mean \pm s.e.m., $n=115$ clusters from nine cells). (G,H) Scatter charts illustrating the positive correlation between T_{ER} and τ_{KV} (G) and the low correlation between τ_{KV} and τ_{ER} (H). The ellipses are 95% confidence intervals based on a linear fit of the data points. (I) Bar graph illustrating the Pearson's correlation coefficients between the lag times, T , and the decay times, τ . * $P<0.01$.

between Kv2.1 and cER decay time, indicating that once the cER started retracting, the rate was independent of Kv2.1 (Pearson's $r=0.04$, Fig. 5I). These data indicate that glutamate exposure results in a dramatic retraction of the cER, which begins once enough Kv2.1 channels have been lost from the clusters.

The role of specific Kv2.1 C-terminal amino acids in ER-plasma-membrane junction formation

The clustering of Kv2.1 is dependent upon the phosphorylation state of a 26-amino-acid sequence on the intracellular C-terminus called the proximal restriction and clustering (PRC) domain (Lim et al., 2000). Removal of the majority of the C-terminus causes a complete abrogation of clustering (Mohapatra and Trimmer, 2006), as do several individual serine point mutations in the PRC (Lim et al., 2000). Because the clustering of Kv2.1 and the remodeling of the cER appear to be inextricable processes, we would expect that any manipulation that disrupts clustering would in turn prevent cER remodeling. Fig. 6A,B illustrates two individual serine-to-alanine point mutants (S583A and S586A) within the PRC that eliminate Kv2.1 clustering and leave the cER with a tubular, mesh-like pattern

that is typical of untransfected HEK cells. Mutation of a single serine residue just outside of the PRC (S603A, Fig. 6C) did not abrogate clustering entirely, but did fail to remodel the cER as dramatically as wild-type Kv2.1, suggesting that the mutation weakened the interaction with the cER. Another domain that is contained within the Kv2.1 C-terminus is the syntaxin binding domain (SBD), which is required for the expression of apoptotic K^+ currents that are carried through Kv2.1 (Leung et al., 2003; McCord et al., 2014). However, removal of the syntaxin binding domain (Δ SBD) did not alter Kv2.1 clustering or cER remodeling (Fig. 6D), indicating that syntaxin binding plays no role in remodeling of the cER.

Ca²⁺ channels localize to the Kv2.1-induced ER-plasma-membrane junctions

Although the function of the Kv2.1-induced ER-plasma-membrane junctions is unknown, junctions that are stabilized by other proteins are most frequently implicated in Ca^{2+} signaling. In many cell types, STIM1 translocates to and enlarges ER-plasma-membrane junctions in response to a drop in ER [Ca^{2+}]. Activated STIM1 in turn binds to and gates plasma membrane Ca^{2+} channels, including ORA1 and members of the transient receptor potential C (TRPC) family, leading to Ca^{2+} flux, ER Ca^{2+} store refilling and transcription factor activation (Hogan et al., 2010). In the presence of Kv2.1 clusters, activated STIM1 molecules translocate to the Kv2.1-induced ER-plasma-membrane junctions where they bind to and localize ORA1 (Fig. 7A–F). Thus, Kv2.1 clusters could be sites of ER Ca^{2+} store or agonist-operated Ca^{2+} entry. In neurons, activated STIM1 binds to and inhibits L-type Ca^{2+} channels (LTCCs) (Park et al., 2010; Wang et al., 2010). In order to determine whether voltage-gated Ca^{2+} channels localize to the Kv2.1-induced ER-plasma-membrane junctions, we co-expressed cyan fluorescent protein (CFP)-tagged Kv2.1 and yellow fluorescent protein (YFP)-tagged Cav1.2 (encoded by *Cacna1c*) in rat hippocampal neurons. Fig. 7G–I shows that Cav1.2 localized to Kv2.1 clusters, suggesting that regulation of voltage-gated Ca^{2+} activity also occurs within these cell-surface domains.

Kv2.1 clusters also represent ER-plasma-membrane junctions within the axon initial segment

Kv2.1 clusters form within the axon initial segment, where localization of voltage-gated Na^+ channels is necessary for the initiation of axon action potentials (Sarmiere et al., 2008). Because Kv2.1 clusters are often adjacent to RyRs at the axon initial segment (King et al., 2014) we examined the relationship between Kv2.1 clusters and the DsRed2-ER marker at the axon initial segment in cultured rat hippocampal neurons, as illustrated in Fig. 8. Here, co-expression of CFP-Nav1.6 (Nav1.6 is encoded by *Scn8a*) was used to identify the axon initial segment, as this is the only process that shows a concentration of Na^+ channels. The colocalization between GFP-Kv2.1 and the DsRed2-ER reporter (Fig. 8) indicates that the Kv2.1 clusters within the axon initial segment represent ER-plasma-membrane junctions that are similar to those on the soma.

DISCUSSION

Although an association between Kv2.1 clusters and the ER has been established (Antonucci et al., 2001; Du et al., 1998; Mandikian et al., 2014), the results presented above indicate that Kv2.1 plays a direct role in forming a membrane contact site (MCS) comprising the cER and plasma membrane. Thus, Kv2.1 is the first plasma membrane protein to be shown to induce these MCSs. This mechanism is in stark contrast to other known ER-plasma-membrane tethering proteins, such as STIM and the extended

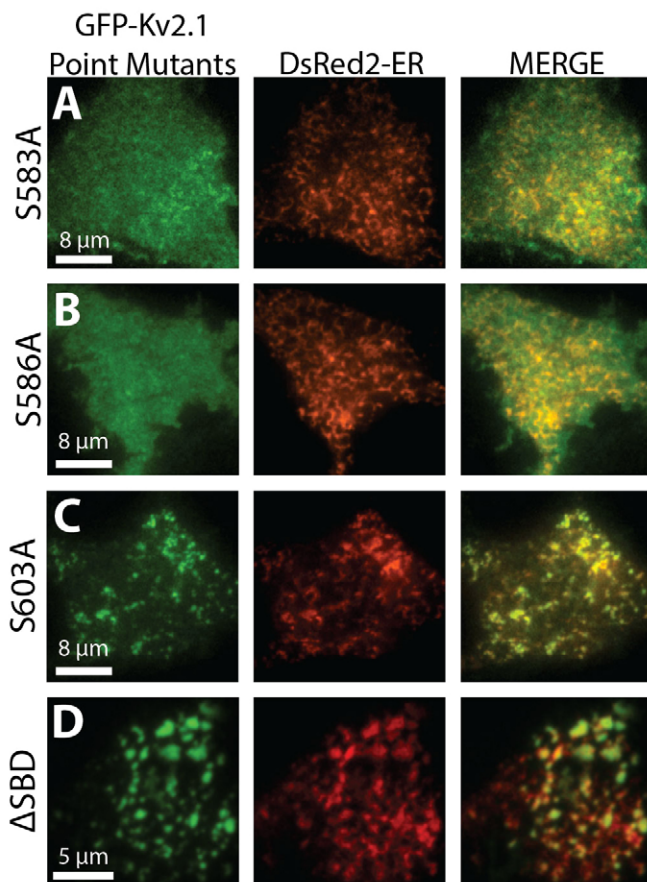


Fig. 6. Both Kv2.1 clustering and remodeling of the cER are disrupted by C-terminal mutations. HEK cells that had been transfected with DsRed2-ER (middle panels) and GFP-fused Kv2.1 mutants (left panels) were imaged in TIRF. (A,B) S583A (A) and S586A (B) are mutations of phosphorylated serine residues located in the proximal regulation of clustering (PRC) domain. These mutants had no effect on the cER and displayed no clustering. (C) S603A is a mutation of a phosphorylated residue just outside of the PRC, and this mutant displayed smaller clusters than wild-type Kv2.1 and didn't remodel the cER as drastically. (D) Δ SBD lacks the Kv2.1 syntaxin binding domain (SBD), Δ 411–522. Δ SBD appeared to form almost wild-type-like clusters and remodeled the cER.

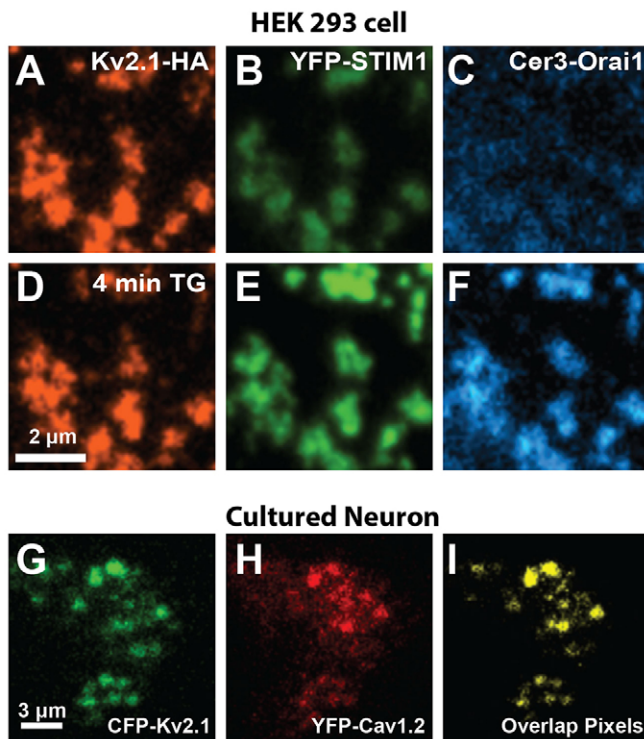


Fig. 7. Localization of Ca^{2+} channels to Kv2.1-induced ER-plasma-membrane junctions. (A–F) A HEK cell that expressed Kv2.1–HA (red), YFP–STIM1 (green) and Cerulean3 (Cer3)–ORAI1 (blue) before (A–C) and after (D–F) treatment with 2 μM Thapsigargin (TG). The Kv2.1 clusters in red colocalized with YFP–STIM1 before treatment with TG owing to the underlying cER, whereas Cer3–ORAI1 was spread diffusely throughout the membrane. After 4 min of TG, the Kv2.1 clusters were essentially unchanged, whereas the intensity of YFP–STIM1 at the Kv2.1-induced ER–plasma-membrane junctions was increased due to the activation and translocation of STIM1. Cer3–ORAI1 became localized to the Kv2.1-induced ER–plasma-membrane junctions through interaction with activated STIM1. (G–I) A 7-DIV-cultured rat hippocampal neuron expressing GFP–Kv2.1 (G, green) and YFP–Cav1.2 (H, red). Clusters of Kv2.1 and Cav1.2 colocalized, and pixels containing both fluorescent signals are displayed in I (yellow).

syntaxins (Carrasco and Meyer, 2011; Giordano et al., 2013), which primarily reside within the ER membrane and are thought to induce junctions by interacting with anionic phospholipids on the inner leaflet of the plasma membrane, often under conditions of ER [Ca^{2+}] depletion. Using both live-cell TIRF imaging and immuno-gold electron microscopy, we show that Kv2.1 expression in HEK cells dramatically increases the amount of cER membrane that is in close (15 nm) proximity to the cell surface. This induction of micron-sized ER–plasma-membrane junctions occurs at rest, in the absence of ER [Ca^{2+}] depletion. Analysis of the temporal relationship between Kv2.1 clustering and cER remodeling, as shown in Figs 3 and 5, suggests that channel clustering and cER interaction are closely linked processes. The role of Kv2.1 in the formation of a MCS is likely to extend to non-neuronal cells, because when GFP–Kv2.1 is expressed in adult atrial myocytes, surface clusters form that appear to be identical to the sarcoplasmic-reticulum–plasma-membrane junctions found in this cell type (O’Connell et al., 2008). By contrast, in adult ventricular myocytes, no plasma membrane Kv2.1 clusters were observed, with the majority of the GFP–Kv2.1 localized to intracellular junctions between the longitudinal and transverse tubule systems (O’Connell et al., 2008).

When using transfected cells there is the concern that overexpression artifacts can occur. However, our previous work

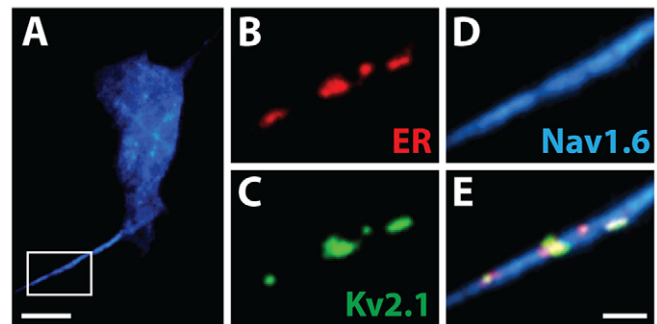


Fig. 8. Kv2.1-induced ER–plasma-membrane junctions are present at the axon initial segment of cultured hippocampal neurons. (A) A representative 12-DIV rat hippocampal neuron that had been imaged in TIRF after transfection with GFP–Kv2.1, DsRed2–ER and Nav1.6–Cerulean3. (B–E) Magnification of the axon initial segment (white box). The ER (B, red) colocalized with Kv2.1 clusters (C, green) in the axon initial segment, which was denoted by the accumulation of Nav1.6–Cerulean3 (D, blue). (E) Overlay image of B–C. Scale bars: 5 μm (A); 2 μm (E).

has demonstrated that expression of exogenous Kv2.1 in HEK cells is similar to the expression of endogenous Kv2.1 in mature cultured hippocampal neurons (2–3 weeks in culture) (Fox et al., 2013b). The average density of Kv2.1 clusters for 20-DIV-cultured rat hippocampal neurons was 58.8 ± 5.4 channels/ μm^2 (s.e.m., $n=10$ cells), whereas the average density of Kv2.1 clusters in a transfected HEK cell at the lower end of the expression spectrum was 63.2 ± 2.8 channels/ μm^2 (s.e.m., $n=13$ clusters). Thus, the minimum density of Kv2.1 channels that is required to form a cluster in HEK cells is very close to the actual density of Kv2.1 channels within endogenous clusters in cultured neurons. Furthermore, the morphological appearance of Kv2.1 clusters in HEK cells and cultured neurons is surprisingly similar to that observed in the intact brain (O’Connell et al., 2006). These data make a strong case that Kv2.1 clustering in HEK cells is not due to overexpression and that this cell system is a good experimental model for Kv2.1 clustering in neurons. In addition, supplementary material Fig. 1 shows that as the endogenous Kv2.1 expression increases with time in culture, the cortical ER morphology, as imaged using TIRF, transitions from the tubular phenotype to that characteristic of Kv2.1-induced ER–plasma-membrane junctions.

Although the existence of the unique Kv2.1 clusters has been known for a long time, the mechanism underlying Kv2.1 clustering has been elusive, especially when considering the unique behavior of channels within the clusters. Clustered channels rapidly diffuse within the interior of the clusters but are confined within the cluster boundary for up to an hour (O’Connell et al., 2006; Tamkun et al., 2007; Weigel et al., 2011). Non-clustered channels can diffuse through the clusters without becoming trapped or being obstructed by the cluster boundary. We postulate that the crucial factor in Kv2.1 retention within the cluster is the binding to an unknown ER factor, whether it be protein or lipid, which is mobile within the ER membrane. Given the known importance of phosphorylation state in the clustering of Kv2.1 (Lim et al., 2000; Misonou et al., 2004; Mohapatra and Trimmer, 2006), it is likely that channels with the proper combination of phosphorylated residues bind to an ER component that in turn prevents them from diffusing away from the cER positioned below. Kv2.1 channels that lack the proper phosphorylation state, and other membrane proteins (Tamkun et al., 2007), move through the cluster without hindrance. The glutamate-induced declustering in Fig. 5 is therefore likely to be due to a calcineurin-dependent dephosphorylation that is caused by

Ca²⁺ influx through extrasynaptic N-methyl-D-aspartate (NMDA) receptors (Misonou et al., 2005; Misonou et al., 2004; Misonou et al., 2008; Mulholland et al., 2008), subsequently freeing the Kv2.1 C-terminus from the cER membrane; allowing channels to diffuse out of the cluster. The time lag between declustering and cER retraction is likely to result from only a fraction of the clustered channels being required to hold the cER membrane at the cell surface.

Although Kv2.1 clusters were initially thought to function as hubs for Kv2.1 regulation, this increasingly appears not to be the case as the regulation of Kv2.1 function is largely independent of channel clustering (Baver and O'Connell, 2012; Fox et al., 2013b). Previous expression studies with Kv2.1 have suggested that the channel might have functions unrelated to K⁺ conductance. Kv2.1 is distinct from other Kv channels in that it is efficiently trafficked to, and abundantly expressed on, the cell surface (Fox et al., 2013b). In addition, a majority of Kv2.1 in both transfected HEK cells and hippocampal neurons exists in a non-conducting state, and induction of this state is dependent on the cell surface density (Fox et al., 2013b; O'Connell et al., 2010). Our current findings – i.e. that Kv2.1 plays a structural role in order to remodel the cER – explain the need for both the high expression and non-conducting state. Given the number of channels that are likely to be required to form the ER–plasma-membrane junctions, evolution of the non-conducting state was essential in order to avoid electrically silencing neuronal activity. Thus, it is unlikely that the function of the Kv2.1-induced ER–plasma-membrane junctions involves Kv2.1 K⁺ conductance. Instead, the localization of both store-operated and voltage-activated Ca²⁺ channels to Kv2.1-induced ER–plasma-membrane junctions (Fig. 7) suggests that these domains are sites for localized Ca²⁺ homeostasis. The finding that RyRs are often adjacent to Kv2.1 on the neuronal soma (Mandikian et al., 2014) further supports this idea. Given that endo- and exocytosis often occur adjacent to the Kv2.1 cluster perimeter (Deutsch et al., 2012), these domains might also link Ca²⁺ signaling to membrane trafficking in both the neuronal soma and axon initial segment.

MATERIALS AND METHODS

Plasmid constructs, cell culture and transfections

Fluorescent-protein-, HA-epitope- and biotin acceptor domain (BAD)-tagged Kv channel constructs have been described previously (O'Connell et al., 2010; O'Connell et al., 2006; O'Connell and Tamkun, 2005; Tamkun et al., 2007) and are based on the Living Colors vector system (Clontech). The HA epitope or BAD sequence was contained within the extracellular domain between the first and second transmembrane domains of Kv2.1 (Tamkun et al., 2007). When necessary, the BirA biotin ligase in the pSec vector was co-transfected with Kv2.1 to achieve biotinylation during channel biosynthesis, presumably within the ER lumen (Tamkun et al., 2007). YFP–STIM1 and Cerulean3–ORAI1 were a gift from Dr Albert Gonzales (University of Vermont, Burlington, VT). GFP–CB5 [the membrane domain of cytochrome B5 (CYB5A) fused to green fluorescent protein] was a gift from Gia Voeltz (University of Colorado, Boulder, CO). YFP–Cav1.2 was a gift from Dr Kurt Beam (University of Colorado-Denver, Aurora, CO). The luminal ER marker pDsRed2-ER was obtained from Clontech (Mountain View, CA).

HEK 293 cells [American Type Culture Collection (ATCC), passage 38–45] cells were transfected using a Bio-Rad GenePulser Xcell (Bio-Rad Laboratories, Hercules, CA) with a 0.2-cm gap cuvette and a single 25-ms pulse of 110-V. The amount of plasmid DNA used in transfection was as follows – 2 µg of Kv2.1 DNA, 200 ng of DsRed2-ER, 300 ng YFP–STIM1, 1.5 µg of Cerulean3–ORAI1, 1 µg of GFP–CB5, 750 ng YFP–Cav1.2 and 1 µg of pSec Bir A. Transfected cells were plated onto glass-bottomed 35-mm dishes (Matek, Ashland, MA) that had been previously coated with Matrigel (BD Biosciences, San Jose, CA) and covered in Dulbecco's modified

Eagles' medium containing 10% fetal bovine serum. HEK cells were imaged within 24 h of electroporation in HEK physiological imaging saline comprising 146 mM NaCl, 4.7 mM KCl, 2.5 mM CaCl₂, 0.6 mM MgSO₄, 1.6 mM NaHCO₃, 0.15 mM NaH₂PO₄, 0.1 mM ascorbic acid, 8 mM glucose and 20 mM Hepes, pH 7.4.

Neurons from cryo-preserved embryonic day (E)18 rat hippocampal dissociations were plated at a density of ~15,000–30,000 cells/cm² on poly-D-lysine-coated glass-bottomed dishes (Matek, Ashland, MA) and cultured in glial-cell conditioned neurobasal medium containing B27 supplement (Life Tech, Carlsbad, CA) as previously described (O'Connell et al., 2006). Animals were deeply anesthetized with isoflurane and euthanized by decapitation according to a protocol approved by the Institutional Animal Care and Use Committee (IACUC) of Colorado State University. Transfections were performed after 6–10 days in culture by using 2.0 µl of Lipofectamine 2000 (Life Tech) using 100 µl OptiMem (Life Tech) according to the manufacturer's directions. At 2 h after transfection, the culture medium was replaced with fresh neurobasal–B27 medium. Neurons were imaged 24–48 h post-transfection in neuronal imaging saline comprising 126 mM NaCl, 4.7 mM KCl, 2.5 mM CaCl₂, 0.6 mM MgSO₄, 0.15 mM NaH₂PO₄, 0.1 mM ascorbic acid, 8 mM glucose and 20 mM HEPES, pH 7.4. Immunostaining of the endogenous Kv2.1 expression in cultured neurons was performed as previously described (Fox et al., 2013b) using a monoclonal antibody against Kv2.1 (clone K89/34, 75-014) from the UC Davis/National Institutes of Health NeuroMab Facility.

Electron microscopy

HEK 293 cells (ATCC, Manassas, VA) at low passage (37–44) were transfected with Kv2.1–HA or no plasmid, fixed with 2.5% glutaraldehyde in 0.15 M Sorensen's phosphate buffer (SPB), pH 7.4, and free aldehydes were quenched with 1% sodium borohydride. Samples were stained using a monoclonal primary antibody against HA (Covance, Princeton, NJ) diluted 1:100 in SPB with 1% IgG and fatty-acid free BSA (Sigma-Aldrich, St Louis, MO). Goat anti-mouse 10-nm and 20-nm-gold-conjugated antibodies were diluted 1:50 (Ted Pella, Redding, CA). Following labeling, cells were post-fixed in osmium tetroxide, en-bloc-stained with uranyl acetate and embedded in alradite-epon. Following thin sectioning, samples were observed on a JEOL 1400 transmission electron microscope. Quantification of gold labeling and ER–plasma-membrane junctions was performed using the ImageJ plugin TrakEM2 (Cardona et al., 2012; Schneider et al., 2012).

TIRF microscopy

The majority of experiments utilizing light microscopy were performed using TIRF microscopy to restrict illumination to within ~100 nm of the basal surface of the cell in order to visualize the cER (Fox et al., 2013a). Transfected HEK cells and neurons were imaged with a Nikon Eclipse Ti Perfect-Focus equipped TIRF/widefield fluorescence microscope equipped with AOTF controlled 405, 488, 543 nm diode lasers, 100 mW each, and an Intensilight wide-field light source. A 100× PlanApo TIRF, 1.49 NA, objective was used for image acquisition. Fluorescent signals were separated using a single quadruple pass dichroic cube (TRF89902-EM, Chroma, Bellows Falls, VT) with excitation bands for 405-, 488-, 561- and 647-nm lasers, and band pass emission filters for blue (450/50), green (525/50), red (605/52) and far red (700/50). Emission was collected and filtered through a Sutter Lambda 10-3 filter wheel containing barrier filters for DAPI (460/50), FITC (535/40), TRITC (620/60) and Cy5 (700/70). The stage and objective were temperature controlled through a Zeiss/Pecon stage heating insert and objective heater at 37°C. Images were captured with the Andor iXon EMCCD iXon DU-897 camera, 512×512 (Andor, Belfast, Northern Ireland). For all imaging experiments, the cells were on the microscope stage for less than 1 h. Perfusion during imaging experiments was gravity fed into a culture dish insert (Wheaton, Millville, NJ) and aspirated by a peristaltic pump to achieve even flow.

Tracking of cER–Kv2.1 clusters

Kv2.1 clusters and associated cER were automatically tracked using a centroid-based algorithm implemented in LabView (National Instruments,

Austin, TX). The images were manually thresholded in order to eliminate background effects, and then the centroid of the structure (X_c, Y_c) was determined from its fluorescence intensity profile:

$$X_c = \frac{\sum_x \sum_y xI(x,y)}{\sum_x \sum_y I(x,y)},$$

and similarly for Y_c , where $I(x,y)$ is the intensity of the image at point (x,y) (Carter et al., 2005).

Particle image velocimetry analysis

HEK cells were transfected with either DsRed2-ER alone or GFP-Kv2.1 and DsRed2-ER, and the DsRed2-ER signal was imaged in TIRF at 31.25 frames per second. The mobility of ER-plasma-membrane junctions in the presence or absence of Kv2.1 channels was analyzed with particle image velocimetry (PIV). PIV is a whole-field technique that employs a cross-correlation algorithm between successive images. We implemented the PIV analysis in MATLAB using the PIVlab toolkit (Thielicke and Stamhuis, 2014). Only one out of every ten frames was used in the PIV processing, providing a time lapse of 0.32 s. Images were converted to 8 bit and then, the local contrast was enhanced in ImageJ with contrast-limited adaptive histogram equalization (CLAHE) (Schneider et al., 2012). We analyzed each frame pair in the PIVlab toolkit with three successive passes employing box sizes of 64×64 , 32×32 and 16×16 pixels with a 50% overlap (pixel size in our images is 158 nm).

Glutamate-induced Kv2.1 declustering

Rat hippocampal neurons were transfected between day DIV 6–10 with GFP-Kv2.1 and DsRed2-ER, and then imaged 24–48 h later. Neurons that expressed both plasmids were imaged in TIRF for 5–10 min before perfusion of 20 μ M glutamate in neuron-imaging saline at room temperature. Glutamate perfusion lasted 30–60 s and then the glutamate solution was allowed to sit in the bath for the remainder of imaging. For intensity measurements, the locations of Kv2.1 clusters were automatically tracked using a centroid-based algorithm implemented in LabView. Intensity measurements were normalized by subtracting the minimum and dividing by the maximum value. Normalized intensities were plotted in Log scale, and the normalized fluorescence decrease was fit using:

$$I(t) = \exp[-(t - T)/\tau],$$

where T is the lag time and τ the characteristic fluorescence decay time. The lag time between glutamate perfusion and fluorescence loss was measured by hand as the point where the linear fit described in the above equation crosses the baseline fluorescence level (dashed lines, Fig. 4E). Pearson's correlation coefficients and P -values were calculated as described previously (Press et al., 2007). Ellipses representing 95% confidence were generated in Origin Pro v8.5.

Image presentation, data analysis and statistics

Images were imported into Velocity 6.1.1 software for object detection, tracking and quantitative analysis. Further tracking and quantification of images was performed in Labview. Numerical data were exported into Origin Pro 8.5 for further analysis and curve fitting. Data are presented as either mean \pm s.d. or mean \pm s.e.m. as indicated in the text. Significance was evaluated using a two-tailed Student's t -test assuming unequal variance for unpaired samples with a P -value cutoff of 0.01.

Acknowledgements

Special thanks go out to Durga Mohapatra (Washington University, St Louis, MO) for providing Kv2.1 point mutants and to Aubrey Weigel for help with data analysis. We also thank Laura Solé and Ben Johnson for review of the manuscript.

Competing interests

The authors declare no competing or financial interests.

Author contributions

P.D.F. designed and performed experiments, analyzed data and wrote the manuscript. C.J.H. and E.J.A. performed experiments and analyzed data. P.J.S. analyzed data. D.K. designed experiments, analyzed data and edited the

manuscript. M.M.T. designed and performed experiments, analyzed data and edited the manuscript.

Funding

This work was supported by the National Institutes of Health [grants R01GM84136 and R01GM084136S1 awarded to M.M.T. and R01GM109888 awarded to M.M.T. and D.K.]. This work was also supported by the National Science Foundation [grant 1401432 awarded to D.K. and M.M.T.]. Deposited in PMC for release after 12 months.

Supplementary material

Supplementary material available online at <http://jcs.biologists.org/lookup/suppl/doi:10.1242/jcs.166009/-/DC1>

References

- Antonucci, D. E., Lim, S. T., Vassanelli, S. and Trimmer, J. S. (2001). Dynamic localization and clustering of dendritic Kv2.1 voltage-dependent potassium channels in developing hippocampal neurons. *Neuroscience* **108**, 69–81.
- Baver, S. B. and O'Connell, K. M. (2012). The C-terminus of neuronal Kv2.1 channels is required for channel localization and targeting but not for NMDA-receptor-mediated regulation of channel function. *Neuroscience* **217**, 56–66.
- Cardona, A., Saalfeld, S., Schindelin, J., Arganda-Carreras, I., Preibisch, S., Longair, M., Tomancak, P., Hartenstein, V. and Douglas, R. J. (2012). TrakEM2 software for neural circuit reconstruction. *PLoS ONE* **7**, e38011.
- Carrasco, S. and Meyer, T. (2011). STIM proteins and the endoplasmic reticulum-plasma membrane junctions. *Annu. Rev. Biochem.* **80**, 973–1000.
- Carter, B. C., Shubeita, G. T. and Gross, S. P. (2005). Tracking single particles: a user-friendly quantitative evaluation. *Phys. Biol.* **2**, 60–72.
- Deutsch, E., Weigel, A. V., Akin, E. J., Fox, P., Hansen, G., Haberkorn, C. J., Loftus, R., Krapf, D. and Tamkun, M. M. (2012). Kv2.1 cell surface clusters are insertion platforms for ion channel delivery to the plasma membrane. *Mol. Biol. Cell* **23**, 2917–2929.
- Du, J., Tao-Cheng, J. H., Zervas, P. and McBain, C. J. (1998). The K⁺ channel, Kv2.1, is apposed to astrocytic processes and is associated with inhibitory postsynaptic membranes in hippocampal and cortical principal neurons and inhibitory interneurons. *Neuroscience* **84**, 37–48.
- English, A. R. and Voeltz, G. K. (2013). Endoplasmic reticulum structure and interconnections with other organelles. *Cold Spring Harb. Perspect. Biol.* **5**, a013227.
- English, A. R., Zurek, N. and Voeltz, G. K. (2009). Peripheral ER structure and function. *Curr. Opin. Cell Biol.* **21**, 596–602.
- Fox, P. D., Haberkorn, C. J., Weigel, A. V., Higgins, J. L., Akin, E. J., Kennedy, M. J., Krapf, D. and Tamkun, M. M. (2013a). Plasma membrane domains enriched in cortical endoplasmic reticulum function as membrane protein trafficking hubs. *Mol. Biol. Cell* **24**, 2703–2713.
- Fox, P. D., Loftus, R. J. and Tamkun, M. M. (2013b). Regulation of Kv2.1 K⁺ conductance by cell surface channel density. *J. Neurosci.* **33**, 1259–1270.
- Franzini-Armstrong, C. and Jorgensen, A. O. (1994). Structure and development of E-C coupling units in skeletal muscle. *Annu. Rev. Physiol.* **56**, 509–534.
- Giordano, F., Saheki, Y., Idevall-Hagren, O., Colombo, S. F., Pirruccello, M., Milosevic, I., Gracheva, E. O., Bagriantsev, S. N., Borgese, N. and De Camilli, P. (2013). PI(4,5)P₂-dependent and Ca²⁺-regulated ER-PM interactions mediated by the extended synaptotagmins. *Cell* **153**, 1494–1509.
- Helle, S. C., Kanfer, G., Kolar, K., Lang, A., Michel, A. H. and Kornmann, B. (2013). Organization and function of membrane contact sites. *Biochim. Biophys. Acta* **1833**, 2526–2541.
- Hogan, P. G., Lewis, R. S. and Rao, A. (2010). Molecular basis of calcium signaling in lymphocytes: STIM and ORAI. *Annu. Rev. Immunol.* **28**, 491–533.
- Kaczmarek, L. K. (2006). Non-conducting functions of voltage-gated ion channels. *Nat. Rev. Neurosci.* **7**, 761–771.
- Kaufmann, W. A., Ferraguti, F., Fukazawa, Y., Kasugai, Y., Shigemoto, R., Laake, P., Sexton, J. A., Ruth, P., Wietzorrek, G., Knaus, H. G. et al. (2009). Large-conductance calcium-activated potassium channels in purkinje cell plasma membranes are clustered at sites of hypolemmal microdomains. *J. Comp. Neurol.* **515**, 215–230.
- King, A. N., Manning, C. F. and Trimmer, J. S. (2014). A unique ion channel clustering domain on the axon initial segment of mammalian neurons. *J. Comp. Neurol.* **522**, 2594–2608.
- Leung, Y. M., Kang, Y., Gao, X., Xia, F., Xie, H., Sheu, L., Tsuk, S., Lotan, I., Tsushima, R. G. and Gaisano, H. Y. (2003). Syntaxin 1A binds to the cytoplasmic C terminus of Kv2.1 to regulate channel gating and trafficking. *J. Biol. Chem.* **278**, 17532–17538.
- Lim, S. T., Antonucci, D. E., Scannevin, R. H. and Trimmer, J. S. (2000). A novel targeting signal for proximal clustering of the Kv2.1 K⁺ channel in hippocampal neurons. *Neuron* **25**, 385–397.
- Mandikian, D., Bocksteins, E., Parajuli, L. K., Bishop, H. I., Cerda, O., Shigemoto, R. and Trimmer, J. S. (2014). Cell type-specific spatial and functional coupling between mammalian brain Kv2.1 K channels and ryanodine receptors. *J. Comp. Neurol.* **522**, 3555–3574.

- McCord, M. C., Kullmann, P. H., He, K., Hartnett, K. A., Horn, J. P., Lotan, I. and Aizenman, E.** (2014). Syntaxin-binding domain of Kv2.1 is essential for the expression of apoptotic K⁺ currents. *J. Physiol.* **592**, 3511-3521.
- Misonou, H., Mohapatra, D. P., Park, E. W., Leung, V., Zhen, D., Misonou, K., Anderson, A. E. and Trimmer, J. S.** (2004). Regulation of ion channel localization and phosphorylation by neuronal activity. *Nat. Neurosci.* **7**, 711-718.
- Misonou, H., Mohapatra, D. P., Menegola, M. and Trimmer, J. S.** (2005). Calcium- and metabolic state-dependent modulation of the voltage-dependent Kv2.1 channel regulates neuronal excitability in response to ischemia. *J. Neurosci.* **25**, 11184-11193.
- Misonou, H., Thompson, S. M. and Cai, X.** (2008). Dynamic regulation of the Kv2.1 voltage-gated potassium channel during brain ischemia through neuroglial interaction. *J. Neurosci.* **28**, 8529-8538.
- Mohapatra, D. P. and Trimmer, J. S.** (2006). The Kv2.1 C terminus can autonomously transfer Kv2.1-like phosphorylation-dependent localization, voltage-dependent gating, and muscarinic modulation to diverse Kv channels. *J. Neurosci.* **26**, 685-695.
- Muennich, E. A. L. and Fyffe, R. E. W.** (2004). Focal aggregation of voltage-gated, Kv2.1 subunit-containing, potassium channels at synaptic sites in rat spinal motoneurons. *J. Physiol.* **554**, 673-685.
- Mulholland, P. J., Carpenter-Hyland, E. P., Hearing, M. C., Becker, H. C., Woodward, J. J. and Chandler, L. J.** (2008). Glutamate transporters regulate extrasynaptic NMDA receptor modulation of Kv2.1 potassium channels. *J. Neurosci.* **28**, 8801-8809.
- Nagy, J. I., Yamamoto, T. and Jordan, L. M.** (1993). Evidence for the cholinergic nature of C-terminals associated with subsurface cisterns in alpha-motoneurons of rat. *Synapse* **15**, 17-32.
- O'Connell, K. M. and Tamkun, M. M.** (2005). Targeting of voltage-gated potassium channel isoforms to distinct cell surface microdomains. *J. Cell Sci.* **118**, 2155-2166.
- O'Connell, K. M., Rolig, A. S., Whitesell, J. D. and Tamkun, M. M.** (2006). Kv2.1 potassium channels are retained within dynamic cell surface microdomains that are defined by a perimeter fence. *J. Neurosci.* **26**, 9609-9618.
- O'Connell, K. M. S., Whitesell, J. D. and Tamkun, M. M.** (2008). Localization and mobility of the delayed-rectifier K⁺ channel Kv2.1 in adult cardiomyocytes. *Am. J. Physiol.* **294**, H229-H237.
- O'Connell, K. M., Loftus, R. and Tamkun, M. M.** (2010). Localization-dependent activity of the Kv2.1 delayed-rectifier K⁺ channel. *Proc. Natl. Acad. Sci. USA* **107**, 12351-12356.
- Orci, L., Ravazzola, M., Le Coadic, M., Shen, W. W., Demaurex, N. and Cosson, P.** (2009). From the cover: STIM1-induced precortical and cortical subdomains of the endoplasmic reticulum. *Proc. Natl. Acad. Sci. USA* **106**, 19358-19362.
- Park, C. Y., Shcheglovitov, A. and Dolmetsch, R.** (2010). The CRAC channel activator STIM1 binds and inhibits L-type voltage-gated calcium channels. *Science* **330**, 101-105.
- Porter, K. R. and Palade, G. E.** (1957). Studies on the endoplasmic reticulum. III. Its form and distribution in striated muscle cells. *J. Biophys. Biochem. Cytol.* **3**, 269-300.
- Press, W. H., Teukolsky, S. A., Vetterling, W. T. and Flannery, B. P.** (2007). *Numerical Recipes: The Art of Scientific Computing*, 3rd edn. Cambridge, MA: Cambridge University Press.
- Prinz, W. A.** (2014). Bridging the gap: membrane contact sites in signaling, metabolism, and organelle dynamics. *J. Cell Biol.* **205**, 759-769.
- Raffel, M., Willert, C. E., Wereley, S. T. and J., K.** (2007). *Particle Image Velocimetry: A Practical Guide*. Berlin; Heidelberg: Springer.
- Rosenbluth, J.** (1962). Subsurface cisterns and their relationship to the neuronal plasma membrane. *J. Cell Biol.* **13**, 405-421.
- Sarmiere, P. D., Weigle, C. M. and Tamkun, M. M.** (2008). The Kv2.1 K⁺ channel targets to the axon initial segment of hippocampal and cortical neurons in culture and in situ. *BMC Neurosci.* **9**, 112.
- Schauder, C. M., Wu, X., Saheki, Y., Narayanaswamy, P., Torta, F., Wenk, M. R., De Camilli, P. and Reinisch, K. M.** (2014). Structure of a lipid-bound extended synaptotagmin indicates a role in lipid transfer. *Nature* **510**, 552-555.
- Schneider, C. A., Rasband, W. S. and Eliceiri, K. W.** (2012). NIH Image to ImageJ: 25 years of image analysis. *Nat. Methods* **9**, 671-675.
- Tamkun, M. M., O'Connell, K. M. and Rolig, A. S.** (2007). A cytoskeletal-based perimeter fence selectively corrals a sub-population of cell surface Kv2.1 channels. *J. Cell Sci.* **120**, 2413-2423.
- Thielicke, W. and Stamhuis, E. J.** (2014). *PIVlab – Time-Resolved Digital Particle Image Velocimetry Tool for MATLAB*.
- Wang, Y., Deng, X., Mancarella, S., Hendron, E., Eguchi, S., Soboloff, J., Tang, X. D. and Gill, D. L.** (2010). The calcium store sensor, STIM1, reciprocally controls Orai and CaV1.2 channels. *Science* **330**, 105-109.
- Weigel, A. V., Simon, B., Tamkun, M. M. and Krapf, D.** (2011). Ergodic and nonergodic processes coexist in the plasma membrane as observed by single-molecule tracking. *Proc. Natl. Acad. Sci. USA* **108**, 6438-6443.